AGU PUBLICATIONS

Geochemistry, Geophysics, Geosystems

RESEARCH ARTICLE
10.1002/2017GC006941

# Uranium isotope evidence for an expansion of marine anoxia during the end-Triassic extinction

**Adam B. Jost[1,2], Aviv Bachan[1], Bas van de Schootbrugge[3], Kimberly V. Lau[1,4], Karrie L. Weaver[1], Kate Maher[1], and Jonathan L. Payne[1]**

[1]Department of Geological Sciences, Stanford University, Stanford, California, USA, [2]Department of Earth, Atmospheric, and Planetary Sciences, Massachusetts Institute of Technology, Cambridge, Massachusetts, USA, [3]Marine Palynology and Paleoceanography Group, Department of Earth Sciences, Utrecht University, Utrecht, Netherlands, [4]Department of Earth Sciences, University of California, Riverside, Riverside, California, USA

**Key Points:**
- We observe a $-0.7‰$ excursion in the uranium isotopic composition of lowermost Jurassic limestone
- The excursion is consistent with a 100-fold increase in the areal extent of anoxic sea floor
- Widespread anoxic conditions likely delayed reef recovery until the mid-late Hettangian

**Correspondence to:**
A. B. Jost,
abjost@mit.edu

**Citation:**
Jost, A. B., A. Bachan, B. van de Schootbrugge, K. V. Lau, K. L. Weaver, K. Maher, and J. L. Payne (2017), Uranium isotope evidence for an expansion of marine anoxia during the end-Triassic extinction, *Geochem. Geophys. Geosyst.*, *18*, doi:10.1002/2017GC006941.

Received 29 MAR 2017
Accepted 12 JUL 2017
Accepted article online 26 JUL 2017

**Abstract** The end-Triassic extinction coincided with an increase in marine black shale deposition and biomarkers for photic zone euxinia, suggesting that anoxia played a role in suppressing marine biodiversity. However, global changes in ocean anoxia are difficult to quantify using proxies for local anoxia. Uranium isotopes ($\delta^{238}U$) in $CaCO_3$ sediments deposited under locally well-oxygenated bottom waters can passively track seawater $\delta^{238}U$, which is sensitive to the global areal extent of seafloor anoxia due to preferential reduction of $^{238}U(VI)$ relative to $^{235}U(VI)$ in anoxic marine sediments. We measured $\delta^{238}U$ in shallow-marine limestones from two stratigraphic sections in the Lombardy Basin, northern Italy, spanning over 400 m. We observe a $\sim 0.7‰$ negative excursion in $\delta^{238}U$ beginning in the lowermost Jurassic, coeval with the onset of the initial negative $\delta^{13}C$ excursion and persisting for the duration of subsequent high $\delta^{13}C$ values in the lower-middle Hettangian stage. The $\delta^{238}U$ excursion cannot be realistically explained by local mixing of uranium in primary marine carbonate and reduced authigenic uranium. Based on output from a forward model of the uranium cycle, the excursion is consistent with a 40–100-fold increase in the extent of anoxic deposition occurring worldwide. Additionally, relatively constant uranium concentrations point toward increased uranium delivery to the oceans from continental weathering, which is consistent with weathering-induced eutrophication following the rapid increase in $pCO_2$ during emplacement of the Central Atlantic Magmatic Province. The relative timing and duration of the excursion in $\delta^{238}U$ implies that anoxia could have delayed biotic recovery well into the Hettangian stage.

## 1. Introduction

Marine anoxia has long been suggested as a kill mechanism for the end-Triassic mass extinction, based largely on increased prevalence of organic-rich black shales, spikes in the abundance of biomarkers for photic-zone euxinia, globally observed positive excursions in the $\delta^{13}C$ composition of marine limestones and organic matter, and an overturn in phytoplankton assemblages [*Hallam*, 1990; *van de Schootbrugge et al.*, 2013]. Yet these existing geochemical data are insufficient to quantify how the global extent of marine anoxia changed through the Triassic-Jurassic transition. Such proxies for local conditions are useful tools for recognizing the presence or absence of anoxic conditions at individual sections, but they cannot easily be extrapolated to quantify global changes in the extent of anoxic bottom waters.

Uranium isotopes ($\delta^{238}U$) in marine carbonates can serve as a proxy for global ocean redox conditions and thereby provide a means of quantifying changes in the extent of anoxic bottom waters across geological time [*Brennecka et al.*, 2011a; *Romaniello et al.*, 2013; *Dahl et al.*, 2014; *Azmy et al.*, 2015; *Elrick et al.*, 2016; *Lau et al.*, 2016, 2017]. In seawater, dissolved uranium is a conservative ion and has a residence time of ~400,000 year [*Dunk et al.*, 2002]. It exists in two redox states: soluble U(VI), which is predominately found as the uranyl ion $UO_2^{2+}$ in aqueous complexes with calcium and carbonate ions in seawater [*Djogić and Branica*, 1991; *Maher et al.*, 2013], and insoluble U(IV), which is reduced and removed within the sediment [*Anderson et al.*, 1989; *Barnes and Cochran*, 1990]. This anoxic sink constitutes 15–25% of the total U outflux from the modern ocean (6–12 $\times$ $10^6$ mol/yr), with a majority of the remaining removed via suboxic (10–60%, 5–25 $\times$ $10^6$ mol/yr) and carbonate (5–30%, 3–13 $\times$ $10^6$ mol/yr) sinks, and alteration of basalt (10–60%,

4–25 $\times$ $10^6$ mol/yr) [*Barnes and Cochran*, 1990; *Morford and Emerson*, 1999; *Dunk et al*., 2002; *Henderson and Anderson*, 2003].

Unlike most lighter isotope systems, uranium isotopes do not experience significant mass-dependent fractionation. Rather, variations in $^{238}U/^{235}U$ arise during reduction of U(VI) to U(IV), where $^{238}U$ is preferentially reduced and removed from solution due to a nuclear volume effect [*Schauble*, 2007]. Little to no uranium isotope fractionation ($\leq$0.1‰) has been observed during weathering or coprecipitation in oxic $CaCO_3$ sediments [*Stirling et al*., 2007; *Weyer et al*., 2008; *Romaniello et al*., 2013; *Andersen et al*., 2016; *Chen et al*., 2016]. Net uranium isotope fractionation in marine sediments reflects preferential reduction of $^{238}U$ over $^{235}U$ as well as the resulting differences in diffusion from the overlying water column into the sediment [*Clark and Johnson*, 2008; *Andersen et al*., 2014]. As a result of these two processes, fractionation in suboxic settings, as opposed to anoxic setting, tends to be low due to low rates of reduction and longer length scales of uranium diffusion [*Andersen et al*., 2014]. Therefore, the proportion of U burial occurring in sediments beneath anoxic bottom waters and the magnitude of fractionation during reduction are the strongest influences on the $\delta^{238}U$ of seawater [*Brennecka et al*., 2011a; *Lau et al*., 2016]. Minor fractionation occurs during adsorption onto ferromanganese crusts (–0.25‰) [*Goto et al*., 2014], but the potential for these sediments to impact seawater on shorter timescales (<1 My) is likely minimal [*Lau et al*., 2017]. Some modern bulk sediments are slightly offset from seawater (+0.2‰), an observation attributed to minor incorporation of U(IV) into the carbonate lattice [*Romaniello et al*., 2013]. Nevertheless, many $CaCO_3$-rich shallow-marine environments are not strongly reducing (they typically have low percentages of total organic carbon [TOC]). Thus, because U(VI) is mostly incorporated into $CaCO_3$ as a trace constituent [*Reeder et al*., 2000, 2004], the $\delta^{238}U$ composition of limestone has the potential to passively track seawater $\delta^{238}U$ and can be used to estimate global fluctuations in the anoxic burial of uranium [*Brennecka et al*., 2011a; *Dahl et al*., 2014; *Elrick et al*., 2016; *Lau et al*., 2016].

The onset of Central Atlantic Magmatic Province (CAMP) volcanism was synchronous with the end-Triassic extinction (ca. 201.6 Ma) [*Blackburn et al*., 2013], suggesting that CAMP emplacement triggered a series of environmental changes that quickly resulted in the loss of major taxonomic groups. Ocean acidification has been proposed as an immediate consequence of volcanism as well as an extinction mechanism for marine organisms [*Hautmann et al*., 2008; *Kiessling and Simpson*, 2011; *Greene et al*., 2012; *Martindale et al*., 2012], but anoxia is also predicted to follow $CO_2$ release. Numerical models of rapid $CO_2$ injection during large igneous province (LIP) volcanism [*Meyer and Kump*, 2008] suggest that both ocean acidification and anoxia are inextricably linked to these types of events. A rapid rise in atmospheric $pCO_2$ initially results in acidification, but as continental weathering subsequently increases in response, so does the delivery of bio-limiting nutrients (e.g., phosphate). This increase in nutrient supply leads to eutrophication, where high phosphate concentrations cause a spike in primary productivity, an increase in amounts of labile organic carbon available for remineralization, and a subsequent drop in seawater $O_2$ and expansion of ocean oxygen minimum zones (OMZs) [*Meyer and Kump*, 2008]. At the same time, higher temperatures caused by increased $pCO_2$ will increase the oxygen demands of most animals [*Bijma et al*., 2013; *Deutsch et al*., 2015] and simultaneously decrease oxygen solubility. Because the synergistic effects of acidification and anoxia may have been particularly deleterious to marine fauna during other periods in Earth history as well [*Pörtner et al*., 2004], particularly the end-Permian extinction [*Knoll et al*., 2007; *Clapham and Payne*, 2011; *Payne and Clapham*, 2012; *van de Schootbrugge and Wignall*, 2015], it critical that we understand both the intensity of these environmental perturbations and timing relative to the end-Triassic extinction event.

In this study, we quantify the increase in the extent of global anoxia across the end-Triassic extinction interval and through the Hettangian (early Jurassic) recovery phase using uranium concentrations and isotopes measured in shallow marine carbonates from two sections in northern Italy. We compare our $\delta^{238}U$ data with other geochemical proxies (namely $\delta^{13}C$, major and trace elements) to help distinguish local effects from global environmental events triggered by the emplacement of CAMP.

## 2. Geologic Setting

The Val Adrara and Italcementi sections are located in the Lombardy Basin of the southern Italian Alps (Figure 1). The two sections are separated by 35 km, with Val Adrara representing a more distal setting on a shallowly dipping, subtidal ramp. The Val Adrara section spans approximately 400 m of stratigraphy,

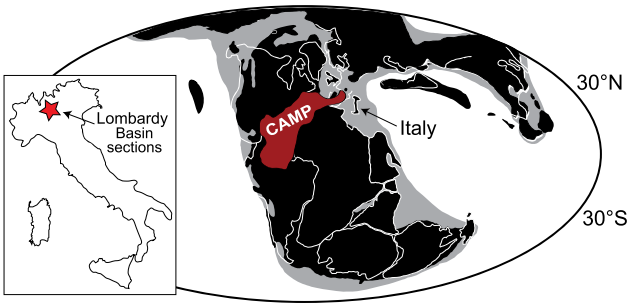


**Figure 1.** Paleogeographic reconstruction ca. 200 Ma showing the aerial extent of CAMP and location of Italy. Inset shows the location of the Lombardy Basin in Italy, where the Val Adrara (45°43′29.33″N, 9°57′32.29″E) and Italcementi (45°46′35.48″N, 9°30′27.09″E) sections are located. Modified from *van de Schootbrugge et al.* [2008] and *Bachan et al.* [2012].

whereas the Italcementi section only spans 100 m, equivalent in age to the lowermost 100 m at Val Adrara. There is no obvious evidence for a protracted depositional hiatus (e.g., karstification and hardgrounds) at either location. Facies successions are similar between the two sections. These sections have been studied previously for sedimentology, paleontology, and $\delta^{13}C$ stratigraphy [see *Bachan et al.*, 2012, and references therein]. Both sections begin in the uppermost Triassic (Rhaetian) Zu limestone, which is composed of algal, molluscan, and coralline packstone and wackestone. Rhaetian fossils (including the Rhaetian pollen taxon *Rhaetipollis germanicus*) last occur in the uppermost Zu limestone and are absent from the overlying Malanotte Formation. At these sections, the Malanotte Formation is interpreted as lowermost Hettangian based on the acme of *Krauselisporites reissingeri* and the accompanying assemblage of other Hettangian-age pollen taxa [*Galli et al.*, 2007]. The base of the Malanotte contains a marl interval, followed by thin-bedded limestones and alternating shales transitioning upward to shallower facies with more abundant bedforms and carbonate grains by the top of the formation [*Bachan et al.*, 2012]. The overlying Albenza Formation comprises peloidal and oolitic packstone and grainstone with infrequent molluscan shells [*Bachan et al.*, 2012]. Both sections contain an abrupt negative $\delta^{13}C$ excursion (N1) immediately above the Triassic/Jurassic (T/J) boundary, followed by an initial minor positive excursion (P1) and a larger, more protracted positive excursion (P2) [*van de Schootbrugge et al.*, 2008; *Bachan et al.*, 2012].

Correlation of the two sections is based primarily on the location of the T/J boundary, which is clearly identified by the transition from the Zu Formation to the overlying Malanotte Fm. [see *Bachan et al.*, 2012]. Further correlations were made by matching trends in $\delta^{13}C$ that are clearly repeated in both stratigraphic sections.

## 3. Geochemical Methods

The methods used in this study are based on the protocols outlined by *Lau et al.* [2016]. We prepared 49 limestone samples for $\delta^{238}U$, [U], and [Th] measurements. Samples were cut with a water saw to remove weathered surfaces. Rock chips of 4–30 g were then broken and powdered in a ceramic mortar and pestle. For uranium isotope measurements, approximately 4 g of powdered rock was digested in 65 mL of 0.25 N HCl to preferentially dissolve the most soluble fraction of $CaCO_3$. Solutions were centrifuged, decanted, dried, and redissolved in 3 mL of concentrated $HNO_3$ and digested overnight at 85°C. Small aliquots (20 μL) of each sample were used to determine [U] for spiking purposes. Samples were then dried again and redissolved in 10 mL of 3 N $HNO_3$, and subsequently a $^{233}U$-$^{236}U$ double-spike tracer was added to obtain a $^{238}U/^{236}U$ of 10. Spiked samples were sent twice through UTEVA resin (Eichrom Technologies) to isolate uranium from other elements in solution. Separated and spiked samples were analyzed on a Nu Plasma high-resolution multicollector inductively coupled plasma mass spectrometer (HR MC-ICPMS) housed at Stanford University. Samples were corrected for mass discrimination and bracketed by solutions of the CRM-145 standard every three samples to correct for instrument drift. Samples are reported using standard delta notation relative to CRM-145 ($^{238}U/^{235}U = 137.844$ [*Condon et al.*, 2010]):

$$\delta^{238}U = \left(\frac{R_{sample}}{R_{CRM-145}} - 1\right) \times 1000, \quad (1)$$

where $R$ is the $^{238}U/^{235}U$ ratio.

Most sample solutions were analyzed at least three times; the average $2\sigma$ for those replicate measurements was 0.11‰. Seven out of 48 samples only yielded enough uranium for two replicate measurements; in

those cases, the 2$\sigma$ is estimated using the reproducibility of the CRM-145 during the appropriate analytical session and averaged 0.15‰ (see Table 1). We analyzed an internal bulk limestone standard (DWP) at −0.23‰ (2$\sigma$ = 0.10, $n$=3), within error of previously published data (–0.27‰ 2$\sigma$ = 0.13, $n$=16 by *Lau et al.* [2016], −0.28‰, 2$\sigma$ = 0.07, n = 3 by *Lau et al.* [2017]). In addition, CRM-129a was analyzed at −1.54‰ (2$\sigma$ = 0.11, $n$ = 10), within error of previously published values (–1.54‰ in *Brennecka et al.* [2010]; −1.52‰ in *Lau et al.* [2017]; −1.53‰ in *Lau et al.* [2017]), though previous studies have suggested that CRM-129a solutions may be heterogeneous [*Andersen et al.*, 2017]. Mean 2$\sigma$ within an individual analysis was 0.08‰.

To determine [U] and [Th] of bulk limestone samples, we dissolved sample powder in 0.5 N HCl overnight to avoid dissolution of noncarbonate phases (e.g., clays, oxides, and organic matter), and subsequently

**Table 1.** Geochemical Data From the Val Adrara and Italcementi Sections[a]

| Stratigraphic Height (m) | $\delta^{13}$Ccarb | $\delta^{18}$O | Ca (wt %) | Mg (wt %) | Sr (ppm) | Mn (ppm) | U (ppb) | Th (ppb) | $\delta^{238}$U | $\delta^{238}$U 2$\sigma$ |
|---|---|---|---|---|---|---|---|---|---|---|
| *Val Adrara* | | | | | | | | | | |
| 2.8 | 1.87 | −2.14 | 31.6 | 0.66 | 656 | 77 | 875 | 201 | −0.07 | 0.10 |
| 9.8 | 2.06 | −2.19 | 31.0 | 0.57 | 929 | 73 | 666 | 209 | −0.41 | 0.21 |
| 20 | 1.36 | −2.26 | 31.3 | 0.67 | 695 | 152 | 927 | 491 | −0.50 | 0.02 |
| 30.8 | 1.41 | −3.52 | 29.7 | 0.66 | 378 | 68 | 1002 | 720 | −0.21 | 0.04 |
| 40 | 2.66 | −2.88 | N/A | N/A | N/A | N/A | 1498 | 117 | −0.27 | 0.16[b] |
| 41.95 | 2.64 | −1.90 | 32.1 | 0.47 | 1204 | 26 | 2051 | 311 | −0.06 | 0.16 |
| 46.9 | 2.54 | −2.02 | 31.4 | 0.55 | 727 | 26 | 1276 | 115 | −0.20 | 0.15 |
| 48 | 2.37 | −2.59 | N/A | N/A | N/A | N/A | 1345 | 246 | −0.28 | 0.05 |
| 51.3 | 1.67 | −3.21 | N/A | N/A | N/A | N/A | 5189 | 177 | −0.02 | 0.13 |
| 53.5 | 2.22 | −2.31 | N/A | N/A | N/A | N/A | 3005 | 149 | −0.19 | 0.06 |
| 57.02 | 2.76 | −2.56 | 33.7 | 0.40 | 2595 | 126 | 760 | 285 | −0.40 | 0.16[b] |
| 57.9 | 3.37 | −1.68 | 34.7 | 0.41 | 2362 | 42 | 521 | 138 | −0.32 | 0.19 |
| 64.7 | 3.79 | −2.11 | 32.3 | 0.43 | 2660 | 74 | 677 | 316 | −0.36 | 0.22 |
| 66.2 | 3.27 | −3.20 | 35.4 | 0.32 | 2386 | 70 | 1143 | 207 | −0.38 | 0.13 |
| 67.7 | 3.06 | −2.94 | 32.9 | 0.31 | 2175 | 87 | 1031 | 273 | −0.43 | 0.08 |
| 71.4 | 3.37 | −2.59 | 33.2 | 0.41 | 1800 | 54 | 1201 | 232 | −0.50 | 0.20 |
| 79 | 3.03 | −3.40 | 35.0 | 0.56 | 896 | 29 | 620 | 145 | −0.44 | 0.04 |
| 86 | 3.15 | −5.84 | 35.4 | 0.66 | 392 | 13 | 442 | 112 | −0.44 | 0.16[b] |
| 95 | 4.40 | −5.32 | 34.4 | 0.16 | 421 | 7 | 742 | 48 | −0.61 | 0.08[b] |
| 100.6 | 4.36 | −5.68 | 33.5 | 1.29 | 460 | 13 | 795 | 57 | −0.49 | 0.17 |
| 108 | 5.02 | −5.40 | 32.7 | 0.63 | 495 | 10 | 777 | 53 | −0.63 | 0.16 |
| 112 | 5.45 | −4.68 | 33.3 | 0.36 | 596 | 8 | 747 | 59 | −0.58 | 0.14 |
| 122 | 5.46 | −4.38 | 32.6 | 0.98 | 425 | 19 | 804 | 60 | −0.54 | 0.14 |
| 135 | 5.21 | −3.83 | 33.6 | 0.12 | 1720 | 23 | 918 | 67 | −0.42 | 0.14 |
| 147 | 5.19 | −4.08 | 32.2 | 0.33 | 835 | 72 | 778 | 66 | −0.57 | 0.10 |
| 175 | 4.76 | −3.33 | 34.1 | 0.18 | 1190 | 6 | 2368 | 366 | −0.51 | 0.11 |
| 200 | 4.17 | −3.92 | 33.4 | 0.29 | 516 | 14 | 697 | 65 | −0.38 | 0.09 |
| 228 | 3.44 | −3.59 | 32.2 | 1.03 | 531 | 14 | 1152 | 97 | −0.43 | 0.16[b] |
| 255 | 1.49 | −4.15 | 30.2 | 2.17 | 737 | 33 | 567 | 108 | −0.26 | 0.16[b] |
| 302 | 1.57 | −4.54 | 27.7 | 4.40 | 364 | 49 | 638 | 207 | −0.24 | 0.20 |
| 356 | 0.51 | −3.75 | 30.4 | 0.47 | 776 | 89 | 523 | 285 | –-0.41 | 0.18[b] |
| *Italcementi* | | | | | | | | | | |
| 7.4 | 2.44 | −1.40 | N/A | N/A | N/A | N/A | 1079 | 272 | −0.30 | 0.12 |
| 23.9 | 2.50 | −1.54 | N/A | N/A | N/A | N/A | 717 | 311 | −0.25 | 0.09 |
| 35.4 | 2.51 | −1.59 | 20.3 | 0.50 | 507 | 513 | 1236 | 226 | −0.09 | 0.05 |
| 41.1 | 2.68 | −4.48 | 31.0 | 0.43 | 623 | 21 | 2917 | 98 | −0.19 | 0.03 |
| 43.1 | 2.42 | −2.91 | 36.0 | 0.30 | 433 | 19 | 2973 | 113 | −0.17 | 0.15 |
| 45.5 | 2.58 | −1.99 | 35.8 | 0.48 | 341 | 21 | 1166 | 957 | −0.13 | 0.13 |
| 47.1 | 3.49 | −1.88 | 26.1 | 0.71 | 624 | 111 | 1673 | 335 | −0.52 | 0.03 |
| 49.9 | N/A | N/A | 44.4 | 0.59 | 3592 | 85 | 1182 | 266 | −0.44 | 0.18 |
| 53 | N/A | N/A | 31.1 | 0.33 | 2173 | 38 | 1127 | 376 | −0.46 | 0.06 |
| 56.6 | 3.68 | −1.92 | 39.8 | 0.41 | 2531 | 59 | 1204 | 329 | −0.42 | 0.06 |
| 61 | 3.73 | −2.19 | 39.8 | 0.36 | 1880 | 74 | 1383 | 440 | −0.38 | 0.06 |
| 65.3 | 3.79 | −2.56 | 31.3 | 0.31 | 1983 | 47 | 961 | 247 | −0.52 | 0.03 |
| 72.9 | 3.35 | −2.14 | 30.4 | 0.31 | 2087 | 50 | 706 | 96 | −0.69 | 0.11 |
| 77 | 3.66 | −2.05 | 35.7 | 0.59 | 1257 | 25 | 784 | 134 | −0.67 | 0.06 |
| 86.5 | 3.83 | −2.58 | 35.8 | 0.45 | 687 | 15 | 437 | 182 | −0.65 | 0.05 |
| 93 | 3.93 | −3.97 | 36.5 | 0.37 | 543 | 13 | 477 | 99 | −0.68 | 0.16 |
| 98.3 | 3.88 | −6.70 | 34.9 | 0.37 | 748 | 7 | 852 | 81 | −0.54 | 0.17 |

[a]For full $\delta^{13}$C data, see *Bachan et al.* [2012, 2014]. Sample external reproducibility is represented by 2 times the standard deviation (2$\sigma$) of repeated measurements from different analytical sessions and is typically less than 0.15‰.

[b]Samples with only two replicate measurements due to low samples size. For these, the 2$\sigma$ is estimated using the reproducibility of the standard during the appropriate analytical session.

centrifuged, decanted, dried, and redissolved the supernatant in 2% $HNO_3$ for analysis on a Nu Plasma AttoM HR ICP-MS also housed at Stanford University. Other geochemical measurements were presented in previously published studies: $\delta^{13}C$ and $\delta^{18}O$ in *Bachan et al.* [2012, 2014]; [Ca], [Mg], [Mn], and [Sr] in *Jost et al.* [2017]. Geochemical data for the samples featured in this study can be found in Table 1.

## 4. Results

The $\delta^{238}U$ records from our two sections are similar where they overlap stratigraphically (Table 1 and Figure 2). The $\delta^{238}U$ values for samples in the uppermost Triassic Zu Formation are variable but generally high (up to $-0.01‰$ at Val Adrara and up to $-0.09‰$ at Italcementi). Two samples in the Zu Fm. at Val Adrara have relatively low values (–0.41 and $-0.50‰$), but similarly low values do not occur at Italcementi in the corresponding interval.

Beginning at the T/J boundary, $\delta^{238}U$ values at both sections begin to decrease, reaching a minimum at the base of the Albenza Formation (of $-0.63‰$ at Val Adrara and $-0.69‰$ at Italcementi). This nadir occurs at the same stratigraphic level at both sections based on correlation via bio-, litho-, and $\delta^{13}C$ chemostratigraphy. Above this level, $\delta^{238}U$ values begin to increase at both sections, although the Italcementi section only captures the very start of this increase before the section ends. At Val Adrara, $\delta^{238}U$ continues to gradually increase to values between $-0.30$ and $-0.25‰$ by 250 m, overlapping the pre-extinction range.

Uranium concentrations in the bulk carbonate are generally $<1200$ ppb throughout the section, with the exception of a substantial increase at the T/J boundary to values upward of 5100 ppb in the upper Zu Formation (Table 1 and Figure 2). Thorium concentrations show a trend similar to that of [U], with most samples $<300$ ppb, but a few samples as high as $\sim$950 ppb in the upper Zu and lowermost Malanotte

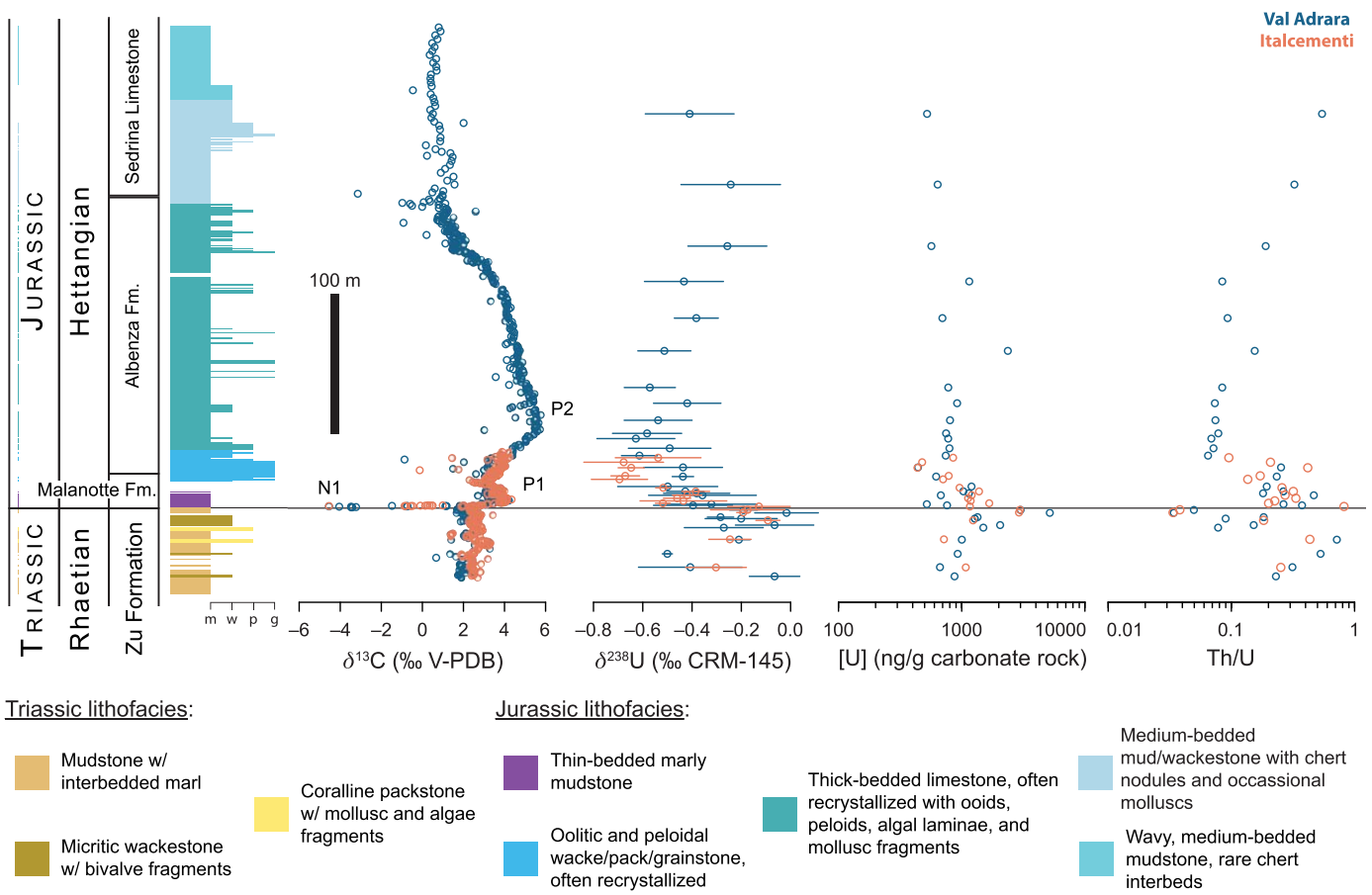


**Figure 2.** $\delta^{13}C$, $\delta^{238}U$, [U], and Th/U data for Val Adrara (blue) and Italcementi (orange). Error bars on $\delta^{238}U$ are $2\sigma$ based on triplicate measurements of the same sample. Lithofacies are based on the Val Adrara section, but facies at Italcementi are very similar where the sections overlap in time. The horizontal black line denotes the T/J boundary.

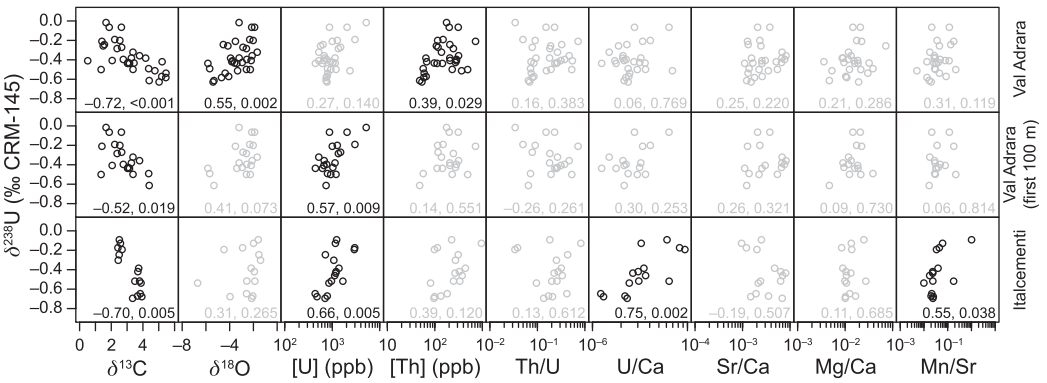


**Figure 3.** Cross plots of major geochemical proxies versus $\delta^{238}$U at Val Adrara (top row), at Val Adrara where it overlaps with Italcementi (middle row), and at Italcementi (bottom row). Spearman's rank values (*p* value, $\rho$) are listed in the corner of each. Black means *p* is significant ($\alpha = 0.05$) and gray means *p* is not significant. $\delta^{13}$C and $\delta^{18}$O values are both shown in ‰ relative to V-PDB.

Formations. Some previous studies on the end-Triassic extinction normalize uranium to thorium as Th/U [*McRoberts et al*., 1997; *Hallam and Wignall*, 2000; *Hallam et al*., 2000; *Wignall et al*., 2007] because detrital U may influence bulk [U] and make it difficult to interpret changes in seawater [U]. However, [U] alone is likely sufficient because our acid dissolution method should only dissolve uranium incorporated into $CaCO_3$ [*Lau et al*., 2016, 2017]. We present both proxy measurements for comparison across studies. Th/U values are highly variable below the Albenza Fm. The lowest Th/U values occur in uppermost Zu formation in both sections (0.03). At Val Adrara, in the lower Albenza, Th/U stabilizes around 0.07 and then gradually increases to 0.50 by the end of the section.

The nadir of the $\delta^{238}$U excursion exists across about 20 m of stratigraphy. The return to higher $\delta^{238}$U values begins 20 m below the maximum $\delta^{13}$C value at this section (the P2 excursion). There is a significant negative correlation between $\delta^{238}$U and $\delta^{13}$C (Spearman's rank: Val Adrara: $\rho = -0.72$, $p = <0.001$; Italcementi: $\rho = -0.70$, $p = 0.005$; Val Adrara first 100 m only: $\rho = -0.52$, $p = 0.019$). Other significant correlations exist in the data, but few are as strong or consistent across sections ($\delta^{238}$U versus $\delta^{18}$O and [Th] at Val Adrara; $\delta^{238}$U versus [U], U/Ca, and Mn/Sr at Italcementi; $\delta^{238}$U versus [U] at Val Adrara first 100 m only). See Figure 3 for all correlation coefficients and cross plots of geochemical data against $\delta^{238}$U.

## 5. Discussion

The protracted negative excursion in $\delta^{238}$U beginning immediately above the T/J boundary at each locality is conceptually consistent with an expansion in ocean anoxia at the end-Triassic mass extinction and corroborates existing lithological and geochemical evidence for increased prevalence of anoxic waters [*Hallam*, 1990; *van de Schootbrugge et al*., 2013]. However, bulk $\delta^{238}$U values in modern Bahamian carbonate sediments are offset from seawater $\delta^{238}$U due to incorporation of reduced uranium [*Romaniello et al*., 2013], suggesting that trends in bulk carbonate $\delta^{238}$U may be influenced by local redox, irrespective of global conditions. Below, we discuss the possible impact of this phenomenon on the $\delta^{238}$U values of our samples and demonstrate that the $\delta^{238}$U excursion in northern Italy cannot fully be explained by this process. We then present a model of the global U cycle to quantitatively constrain the changes in seawater $\delta^{238}$U and [U] during and after the end-Triassic extinction.

### 5.1. Considering Potential Diagenetic Effects on $\delta^{238}$U

Primary marine calcite and aragonite precipitates (e.g., corals, molluscs, calcareous algae, ooids) from modern field settings do not fractionate uranium isotopes during precipitation, and therefore have $\delta^{238}$U values similar to the $\delta^{238}$U of seawater [*Romaniello et al*., 2013]. *Chen et al*. [2016] observed a fractionation of around $+0.1‰$ in inorganic aragonite at pH 8.5. They hypothesize that this is due to equilibrium fractionation among dissolved U(VI) species, but it is not clear whether this fractionation should also be expected in biogenic aragonite given that organisms often modify water chemistry at the site of calcification. Bulk carbonate sediment $\delta^{238}$U is often 0.2–0.4‰ higher than seawater $\delta^{238}$U, likely because uranium is sometimes reduced and fractionated within pore fluids and incorporated in bulk samples, either by incorporation into

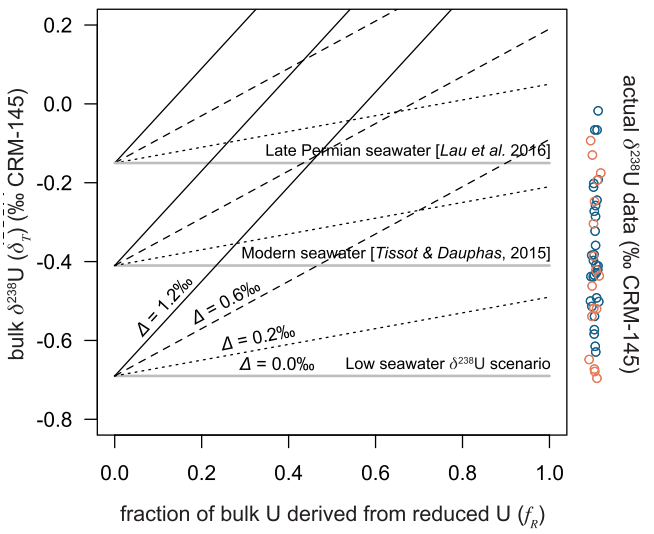


**Figure 4.** Modeled values for bulk $\delta^{238}$U ($\delta_T$) given hypothetical fractions of reduced U ($f_R$) in our samples. Model lines are drawn for three different seawater $\delta^{238}$U compositions (–0.15, −0.41, and −0.69‰) and four different effective (net) fractionations (+0.0, +0.2, +0.6, and +1.2‰). On the right is our actual $\delta^{238}$U data (blue is Val Adrara and orange is Italcementi), offset slightly from center to better show data in dense areas.

the crystal lattice of $CaCO_3$ cements, adsorption to clays or organic matter, or precipitation as finely disseminated authigenic minerals (e.g., uraninite) [*Romaniello et al*., 2013]. Additionally, while fractionation during biotic uranium reduction is observed to be near +1‰ [*Basu et al*., 2014; *Stirling et al*., 2015; *Stylo et al*., 2015] (also see *Andersen et al*. [2014, and references therein] for discussion of theoretically estimated fractionations up to +1.2‰), deposition rate and dissolved $O_2$ concentrations can impact the effective (net) fractionation of bulk reduced uranium [*Andersen et al*., 2014]. In theory, facies differences among ancient carbonate rocks may yield differences in the amount and isotopic composition of reduced uranium, allowing bulk $\delta^{238}$U and [U] to vary independently from global seawater composition.

To test the extent to which variation in the proportion of incorporated reduced uranium can explain the trends in $\delta^{238}$U within our studied stratigraphic sections, in the event that the $\delta^{238}$U of seawater was invariant, we use a simple mixing model,

$$U_T\delta_T = U_C\delta_C + U_R\delta_R, \tag{2}$$

where $U$ is uranium concentration and $\delta$ is the $\delta^{238}$U value for the primary carbonate ($C$), the reduced uranium ($R$), and the total bulk rock ($T$). Assuming that seawater $\delta^{238}$U was constant that primary carbonate was directly recording seawater $\delta^{238}$U values and that $\delta_C$ and $\delta_R$ are offset by the effective uranium reduction fractionation factor ($\Delta$), we can calculate the proportion of reduced uranium ($f_R$) required to account for the $\delta_T$ of each sample

$$f_R = \frac{\delta_T - \delta_C}{\Delta}. \tag{3}$$

During early diagenesis, remineralization of organic matter can result in anoxic pore waters, causing reduction of soluble U(VI) to insoluble U(IV). The effective (net or bulk) fractionation factor observed between bulk reduced U and seawater is typically +0.6‰, approximately half of the intrinsic (instantaneous) fractionation of +1.2‰ [*Clark and Johnson*, 2008; *Andersen et al*., 2014]. The smaller effective fractionation occurs because as $^{238}$U is preferential reduced over $^{235}$U, more $^{238}$U than $^{235}$U diffuses into the sediment column, thereby increasing the $\delta^{238}$U value of U in sediment pore waters and any subsequently reduced uranium. This scenario assumes quantitative reduction in a sediment column where euxinic conditions prevail at the sediment-water interface; in a more oxygenated setting where uranium reduction begins some distance below the sediment-water interface, effective fractionation will approach 0‰ as reduction is quantitative but uranium diffusion is minimal [*Clark and Johnson*, 2008; *Andersen et al*., 2014]. Effective fractionation may be greater than +0.6‰ if uranium reduction is not quantitative, though this would also imply less reduced uranium and thus a smaller impact on bulk $\delta^{238}$U [*Andersen et al*., 2014]. In all cases, the $\delta^{238}$U of the reduced uranium in authigenic components would be higher than the pore water $\delta^{238}$U and the primary $CaCO_3$ $\delta^{238}$U. Therefore, the bulk sediment $\delta^{238}$U would reflect the weighted average of the primary $CaCO_3$ and reduced authigenic uranium, and tend to be higher than contemporaneous seawater $\delta^{238}$U. We assume no additional contributions from detrital, nonauthigenic sources of uranium. We evaluate our mixing model using $\Delta$ values of +0.2, +0.6, and +1.2‰ and a variety of seawater $\delta^{238}$U values to evaluate the likelihood that reduced uranium contamination impacted our record.

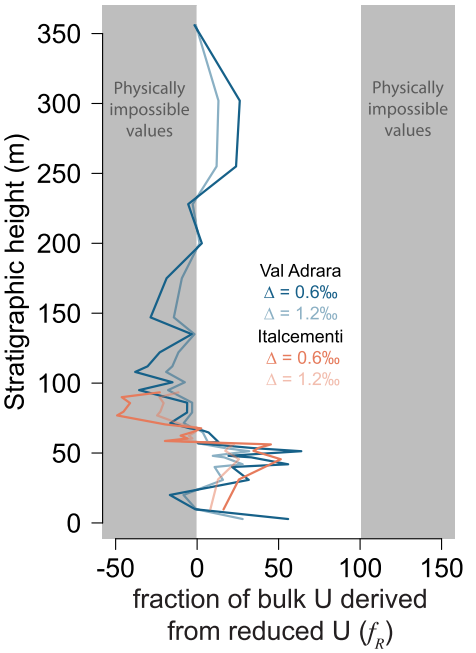


**Figure 5.** We use sample $\delta^{238}$U and [U] values and a mixing model to theoretically estimate how much of the bulk uranium ($f_R$)would need to be comprised of reduced uranium to explain our stratigraphic $\delta^{238}$U trend. Blue is Val Adrara and orange is Italcementi. Models assume a modern seawater $\delta^{238}$U of $-0.41‰$. Darker shades assume an effective fractionation of $0.6‰$ and lighter shades assume $1.2‰$. Gray regions represent bulk fractions less than 0% or greater than 100%, neither of which are physically possible.

Our model assumes that only U(IV) is incorporated into bulk sediments during diagenesis. In theory, distilled U(VI)—fractionated U(VI) left over in the pore water after partial reduction of the initial U(VI) pool—could also be incorporated into bulk samples after burial. This pool would tend to be isotopically similar to seawater during earliest diagenesis and become progressively depleted in $^{238}$U as reduction proceeds. Incorporation of U(VI) would minimize the impact of mixing with enriched reduced uranium. Therefore, our model results represent upper limits for $\delta_T$ at each given $f_R$.

Figure 4 illustrates how the bulk $\delta^{238}$U ($\delta_T$) can vary as a function of $f_R$ assuming a modern seawater $\delta^{238}$U value (–0.41‰ [*Andersen et al.*, 2014; *Tissot and Dauphas*, 2015]), a proposed Late Permian value (–0.15‰ [*Lau et al.*, 2016]), and a hypothetical low value (–0.69‰, equivalent to the lowest value in our data set). The third scenario would require that the baseline extent of anoxic U deposition was occurring over about 3% of the seafloor (15-fold higher than the modern value of ~0.1% [*Helly and Levin*, 2004]) and that seawater [U] was ~1 ppb, all other fluxes being equivalent to modern. We also include our actual $\delta^{238}$U data alongside the modeled values of $f_R$ and $\delta_C$. Figure 5 illustrates a stratigraphic record of calculated $f_R$ values needed to explain our data, assuming a modern seawater $\delta^{238}$U value and fractionations of $+0.6$ and $+1.2‰$.

Because our model only considers that U(IV) with $\delta^{238}$U values greater than contemporaneous seawater is incorporated during early diagenesis, only bulk $\delta^{238}$U values higher than contemporaneous seawater can be explained by mixing with U(IV), regardless of which $\Delta$ or seawater $\delta^{238}$U value is used (Figures 4 and 5). In the case of seawater $\delta^{238}$U equal to $-0.69‰$, it does become theoretically possible to explain the entire range of measured values by mixing with reduced U; however, this would then require that over 50% of bulk U be derived from reduced U and that effective fractionation was at least $+0.6‰$, if not higher. Figure 5 demonstrates that only the lower stratigraphic interval and data between 250 and 300 m is possible according to our model; in particular, the spike in [U] and high $\delta^{238}$U in the latest Triassic may be due to higher amounts of TOC and significant contributions of reduced uranium. Importantly, though, this finding is not evidence for the influence of fractionated U(IV) in and of itself, it merely demonstrates that such a scenario is possible.

Bulk $\delta^{238}$U values less than that of seawater are much more difficult to explain through diagenetic processes than through increasingly anoxic seawater. Some studies have identified bulk carbonate samples with $\delta^{238}$U values lower than modern seawater $\delta^{238}$U [*Romaniello et al.*, 2013; *Hood et al.*, 2016]; however, the mechanism responsible for these observations is not currently known. Abnormally low values may be related to pore-fluid evolution [*Hood et al.*, 2016], dolomitization [*Romaniello et al.*, 2013], or adsorption onto particulate organic matter [*Hinojosa et al.*, 2015; *Holmden et al.*, 2015]. In theory, if pore water reduction of uranium occurs, but only $^{238}$U-depleted U(VI) is incorporated into the bulk sediment, it could decrease the bulk sediment $\delta^{238}$U. However, progressively lower bulk $\delta^{238}$U values become more difficult to explain through this process because the concentration of pore water U(VI) decreases rapidly, thus weakening the influence of this component on bulk $\delta^{238}$U. Consequently, we view this scenario as an unlikely means of generating bulk $\delta^{238}$U values lower than seawater $\delta^{238}$U.

Similarly, incorporation of $^{238}$U-depleted U(VI) is incapable of explaining bulk $\delta^{238}$U values higher than seawater $\delta^{238}$U. Like in the previous scenario, distillation of U(VI) in the pore fluid during diagenesis could

explain our data if seawater $\delta^{238}$U was much higher than at present ($\sim 0‰$ or higher); however, this scenario would require either very high riverine $\delta^{238}$U or an increase in processes that preferentially remove $^{235}$U from the oceans, such as adsorption of uranium onto Mn-oxyhydroxides [*Brennecka et al*., 2011b]. Riverine $\delta^{238}$U values exceeding $0‰$ are theoretically possible if weathered U was sourced entirely from shales or coal, but riverine $\delta^{238}$U values above $-0.2‰$ are rare in the modern world [*Tissot and Dauphas*, 2015]. Likewise, even if ferromanganese crusts were more prevalent during the earliest Jurassic, the fractionation is too small to have significant leverage on seawater $\delta^{238}$U [*Lau et al*., 2017]. Therefore, we view it as unlikely that seawater $\delta^{238}$U was significantly higher than $0‰$ and argue that distillation could not have played a significant role in driving the bulk $\delta^{238}$U of our samples.

Although there exist several diagenetic mechanisms that can, in theory, explain our entire bulk $\delta^{238}$U record, each require unrealistic assumptions, such as very large and varying proportions of reduced uranium or extremely high or low seawater $\delta^{238}$U. Next, we explore the possibility for temporal variation in the $\delta^{238}$U of seawater due to fluctuations in global deposition of U under anoxic bottom waters as an explanation for the $\delta^{238}$U excursion at the Val Adrara and Italcementi sections. In addition, we consider alternative, non-diagenetic, explanations for the $\delta^{238}$U excursion, including changes in mineralogy and in the riverine flux of uranium. We outline a numerical model of the uranium cycle and compare modeling results with our data in an effort to quantify temporal variation in the extent of anoxic bottom waters during and after the end-Triassic extinction event.

### 5.2. Modeling Changes in Seawater $\delta^{238}$U

A negative excursion in $\delta^{238}$U can indicate an increase in the extent of seafloor anoxia and the burial of reduced U. In seafloor sediments, uranium can be quantitatively removed from anoxic sediment pore waters [*Anderson et al*., 1989; *Barnes and Cochran*, 1990]. Therefore, to increase the anoxic uranium burial flux, the area of the seafloor covered by anoxic bottom waters must increase. In the modern ocean, anoxic bottom waters overlie approximately 0.2% of the sea floor [*Helly and Levin*, 2004], yet this small area accounts for approximately 15% of total uranium removal from seawater [*Morford and Emerson*, 1999]. Assuming that uranium buried in the upper sediment column of anoxic localities is fractionated from seawater by an average of $+0.6‰$ [*Andersen et al*., 2014], a relative increase in anoxic uranium deposition will cause the $\delta^{238}$U of seawater to decrease.

To better assess whether our T/J $\delta^{238}$U record reflects an increase in seafloor anoxia, we use a forward model of the uranium cycle outlined by *Lau et al*. [2016]. Uranium input to the oceans is dominated by the riverine flux, while output occurs primarily in anoxic, suboxic, and oxic marine sediments [*Morford and Emerson*, 1999], such that

$$\frac{dM_U}{dt} = F_{riv} - F_{oxic} - F_{suboxic} - F_{anoxic}, \tag{4}$$

where $M_U$ is the number of moles of uranium in the ocean and F is a flux in mol/yr. Removal into suboxic sediments affects seawater [U], but does not cause significant uranium fractionation [*Weyer et al*., 2008]. We can simplify this equation by combining $F_{oxic}$ and $F_{suboxic}$ into one term, $F_{other}$,

$$\frac{dM_U}{dt} = F_{riv} - F_{other} - F_{anoxic}. \tag{5}$$

Burial fluxes scale to the concentration of U in seawater and the areal fraction of uranium deposition, following the form of

$$F = fkM_U, \tag{6}$$

where f is the seafloor areal extent of deposition and k is the scaling coefficient given the initial flux during steady state. The isotope mass balance is calculated using

$$\frac{M_U d\delta_{sw}}{dt} = F_{riv}(\delta_{riv} - \delta_{sw}) - F_{other}(\Delta_{other}) - F_{anoxic}(\Delta_{anoxic}), \tag{7}$$

where $\delta_{sw}$ and $\delta_{riv}$ are the $\delta^{238}$U values of seawater and the riverine input flux, respectively, and $\Delta_{anoxic}$ and $\Delta_{other}$ are the average fractionation factors associated with the anoxic and combined oxic-suboxic output fluxes. Initial parameter values are listed in Table 2. We utilize flux values from Morford and Emerson

**Table 2.** Initial Model Parameters

| | | |
|---|---|---|
| $V_{oc}$ | Ocean volume | $1.41 \times 10^{21}$ L |
| $M_U$ | Moles of U in seawater | $1.96 \times 10^{13}$ mol |
| $F_{riv}$ | Riverine flux of U | $0.4 \times 10^{8}$ mol/yr |
| $f_{anoxic}$ | Initial extent of ocean floor where anoxic U burial occurs | 0.0021 |
| $k_a$ | Anoxic burial scaling coefficient | $1.458 \times 10^{-4}$ |
| $k_o$ | "Other" burial scaling coefficient | $1.738 \times 10^{-6}$ |
| $\delta_{riv}$ Permian | Riverine U isotopic composition | $-0.04‰$ |
| $\delta_{riv}$ modern | Riverine U isotopic composition | $-0.27‰$ |
| $\Delta_{other}$ | Fractionation between seawater and "other" U burial flux | $0.03‰$ |

[*Morford and Emerson*, 1999]; the uncertainty regarding the sizes of the fluxes has a greater effect on the modeled area of anoxic seafloor when $\delta^{238}$U values are very negative (near $-1.0‰$) [*Lau et al*., 2017].

Model and perturbation duration are important factors in predicting $\delta^{238}$U and [U] patterns. Given the long residence time of uranium ($\sim$490 kyr in our model), longer perturbations of low severity may yield $\delta^{238}$U excursions similar in magnitude to those formed from shorter events of greater severity, and in the absence of any age constraints these scenarios are not easily distinguishable.

Absolute age constraints above the T/J boundary at our localities are poor. The upper portion of the Sedrina Limestone at Val Adrara is assigned to the upper Hettangian based on an occurrence of *S. angulata* [*Bachan et al*., 2012, and references therein]. This interpretation implies that the Jurassic stratigraphy at Val Adrara represents near 1 Myr based on duration estimates of ammonite biozones by *Ruhl et al*. [2010]. Other age estimates come from a comparison of our $\delta^{13}$C record with the rises in $pCO_2$ inferred from carbon isotopes in pedogenic carbonate by *Schaller et al*. [2011, 2012]. *Bachan and Payne* [2015] correlated the $\delta^{13}$C record to each of the four separate rises in $pCO_2$ observed by *Schaller et al*. [2011, 2012] using a model of the carbon cycle. *Bachan and Payne* [2015] use these correlations to demonstrate that the entirety of the Val Adrara section above the T/J boundary represents approximately 840 kyr, the duration of CAMP volcanism [*Schaller et al*., 2012]. Alternatively, if the entire $\delta^{13}$C record at Val Adrara was associated with the first two pulses of $CO_2$ only, the same interval would represent approximately 620 kyr. Model results are comparable under both end-member model durations. We opt for 840 kyr as our best estimate because it is similar to the estimate from ammonite biostratigraphy, and approximate 70 kyr for the latest Triassic interval of our study sections by extrapolation assuming constant deposition rate. See below for discussion of longer event durations.

Our preextinction $\delta^{238}$U values are similar to those of the latest Permian, so we assume a Late Permian seawater $\delta^{238}$U composition for our model (–0.15$‰$ [*Lau et al*., 2016]), and generate an increase in anoxia that matches the rate and magnitude of the observed $\delta^{238}$U excursion. *Lau et al*. [2016] attribute these high seawater $\delta^{238}$U values in the late Triassic to higher proportions of shales and organic-rich sediments on the continents available for weathering. Because the excursion at Italcementi appears to occur slightly before the excursion at Val Adrara, based on correlation of $\delta^{13}$C records, the duration of the event and increase in the extent of anoxic deposition should be viewed as a minimum and maximum estimate, respectively. The cause for the difference in timing is unclear, but the difference is most likely due to small differences in depositional rate between the two sections. The magnitude of change in anoxic extent determines the slope of the modeled $\delta^{238}$U and [U] excursions, whereas the duration affects the time at which the excursions turn back toward baseline values. The change in anoxic extent is modeled as an instantaneous shift.

Using these parameters, we can simulate a $0.54‰$ negative $\delta^{238}$U excursion (–0.15 to $-0.69‰$) by increasing anoxic extent ($f$) by a factor of 75 for 44 kyr (Figure 6). The subsequent recovery from this perturbation is more protracted due to the long residence time of uranium in seawater, allowing us to match the observed duration of the excursion with a perturbation of substantially shorter duration. Doing so results in a drawdown of [U] in $CaCO_3$ from 1000 to 390 ppb. This pattern is different from the observed increase from about 875 ppb up to nearly 5200 ppb followed by nearly constant values around 850 ppb. This misfit suggests that our modeled scenario is incomplete.

One possible cause of this misfit is that there was a switch from calcite to aragonite as the dominate polymorph of $CaCO_3$, as aragonite has a larger distribution coefficient than calcite for U [*Reeder et al*., 2000] and also, possibly, a minor isotopic fractionation of $+0.1‰$ [*Chen et al*., 2016]). For the model, we assume a

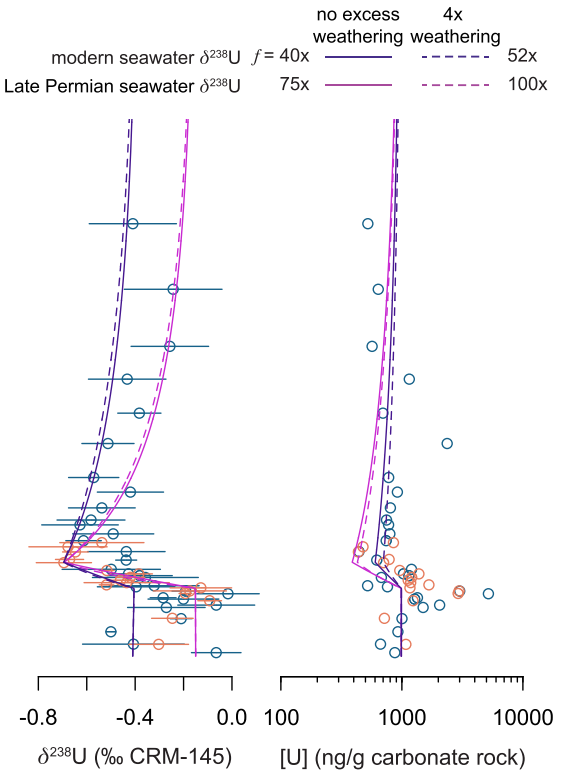


**Figure 6.** $\delta^{238}$U and [U] data overlain with model results for increased extent of anoxic deposition of uranium. All model excursions begin at the T/J boundary and persist for 44 kyr. Violet is for models where the assumed baseline seawater $\delta^{238}$U was $-0.41‰$, while magenta is for models that assume seawater $\delta^{238}$U was $-0.15‰$. The solid violet line represents a 40X increase in anoxia; dashed violet is 52X anoxia and 4X uranium riverine flux; solid magenta is 75X anoxia; dashed magenta is 100X anoxia and 4X riverine flux.

distribution coefficient for calcite ($D_{cal}$) equal to 0.3. Low calcium isotope values and high strontium concentrations at the same localities suggest that a brief interval immediately above the boundary was mostly aragonite in original mineralogy, possibly due to high seawater carbonate saturation levels during recovery from ocean acidification [*Jost et al*., 2017]. Aragonite incorporates more Sr and fractionates calcium isotopes from seawater to a larger degree than calcite does. This increase in the proportion of aragonite could have contributed to the observed changes in [U] and U/Ca; however, the high [Sr] and low calcium isotope values indicate aragonite just above the T/J boundary, whereas the highest uranium concentrations appear below it. Additionally, [U] and U/Ca values are significantly positively correlated with $\delta^{238}$U values at Italcementi and [U] only in the first 100 m of Val Adrara. Together, these observations point toward addition of reduced and fractioned U as the cause of higher [U] rather than a temporary shift to aragonite precipitation.

In either case, there is no satisfactory explanation for the misfit between the nearly constant Jurassic [U] values and the modeled decrease in [U] that occurs simultaneously with the modeled $\delta^{238}$U excursion. One possible avenue to reconciling this discrepancy is a scenario in which increased anoxia was associated with an increase in U delivery via continental weathering. This scenario is consistent with Earth systems modeling, which suggests that anoxia is triggered by an increase in the weathering of nutrients into the ocean [*Meyer and Kump*, 2008]. Based on the $\delta^{13}$C record at our localities, *Jost et al*. [2017] estimated that silicate weathering rates increased by a factor of $\sim$4. An increase in weathering may explain the positive correlation between $\delta^{238}$U and [Th] in our Val Adrara section (Figure 3). We incorporate this weathering change into our model by increasing the uranium riverine flux, though this higher flux also increases the $\delta^{238}$U value of seawater slightly, so a greater change in anoxia is required to generate the same size $\delta^{238}$U excursion. Increasing U weathering fourfold and increasing anoxic extent 100-fold (i.e., to 20% of the seafloor) yields a similar $\delta^{238}$U as before, but the [U] nadir is only increased to 430 ppb. While increasing U weathering does attenuate the predicted decrease in [U], it is insufficient to match the observed changes in [U] and we must therefore explore alternative explanations.

It is possible that the Late Permian $\delta^{238}$U value (–0.15‰) is too high to be representative of the Late Triassic. If we assume that seawater was $-0.15‰$ and that baseline anoxic extent was equivalent to modern (0.21%), then the $\delta_{riv}$ must have been around $-0.04‰$, which is 0.23‰ higher than modern. This value would require that a significant proportion of weathered U be derived from organic rich rocks, such as coal and shale [*Lau et al*., 2016]. While weathering rates likely increased, it is not likely that the proportion of weathered material shifted so strongly toward organic materials, and thus would be a problematic assumption for our model. Therefore, we try to model an excursion where the seawater $\delta^{238}$U was equal to the modern value (–0.41‰ [*Tissot and Dauphas*, 2015]) and assume that any $\delta^{238}$U values greater than seawater are due to the addition of reduced U from diagenetic or authigenic phases to our samples. This is not to say that samples with $\delta^{238}$U values less than contemporaneous seawater $\delta^{238}$U are not influenced by mixing

with reduced uranium, but given the low apparent levels of TOC in the lower Jurassic lithofacies (Figure 2), we assume that the negative $\delta^{238}$U excursion is not significantly impacted by such low TOC concentrations.

Using a modern seawater $\delta^{238}$U value as the baseline and a 40-fold increase in anoxic extent for 44 kyr, our model predicts a $\delta^{238}$U excursion similar to what is observed and a transient decrease in [U] from 1000 ppb to 600 ppb (Figure 6). We can minimize this decrease in [U] by increasing uranium weathering fourfold and increasing the anoxic extent 52-fold. This model scenario increases the [U] nadir to 700 ppb and yields the best match in [U] so far (Figure 6).

Our model assumes that the Jurassic deposits at Val Adrara represent 840 kyr based on correlation with well-dated deposits in the Newark basin [*Schaller et al.*, 2012] (see discussion above). If we relax all age assumptions, we can determine the minimum necessary increase in anoxia by modeling a permanent increase in anoxic extent that generates the observed excursion magnitude (i.e., we calculate a steady state solution). The difference in results arises because in the dynamic model, large changes in extent of seafloor anoxia may yield smaller magnitude $\delta^{238}$U excursions if events are sufficiently short and steady state is never achieved. If we assume a Late Permian seawater $\delta^{238}$U value (–0.15‰), a permanent 24-fold increase in anoxic deposition would shift seawater to −0.69‰. Only a ninefold increase is required if we assume a modern $\delta^{238}$U value (–0.41‰) for Late Permian seawater. Therefore, our most conservative estimate is that the global extent of seafloor anoxia increased by ninefold.

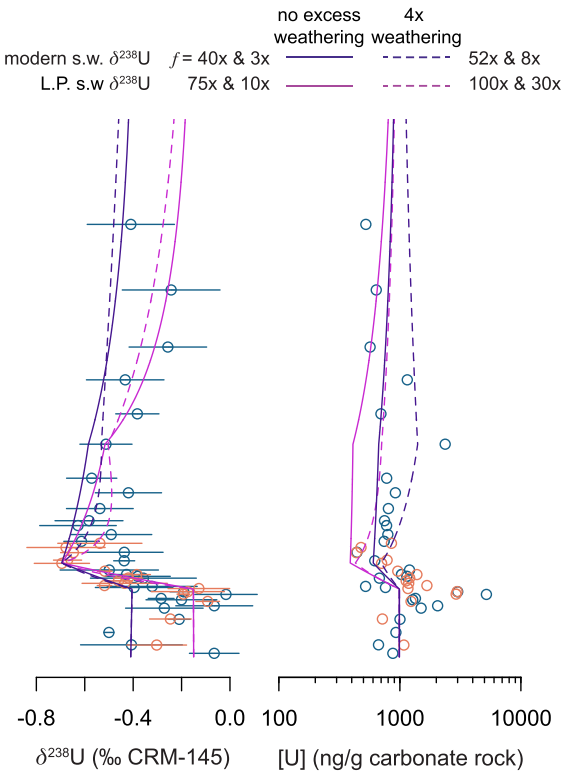


**Figure 7.** $\delta^{238}$U and [U] data overlain with model results for increased extent of anoxic deposition of uranium with a second smaller and more protracted anoxic depositional period. All model excursions begin at the T/J boundary, endure a main anoxia phase for 44 kyr, and then endure a second phase of more limited anoxia for 200 kyr. Violet is for models where the assumed baseline seawater $\delta^{238}$U was −0.41‰, while magenta is for models that assume seawater $\delta^{238}$U was −0.15‰. The solid violet line represents a 40X increase in anoxia followed by 3X anoxia; dashed violet is 52X anoxia followed by 8X anoxia with a 4X uranium riverine flux for the duration of both anoxic events; solid magenta is 75X anoxia followed by 10x anoxia; dashed magenta is 100X anoxia followed by 30X anoxia with a 4X uranium riverine flux for the duration of both events.

In principle, there are several other ways in which one can model a negative $\delta^{238}$U excursion without invoking anoxia. Decreasing riverine $\delta^{238}$U to −3.7‰ would recreate the magnitude of the excursion in seawater $\delta^{238}$U, but it produces no change in [U] and requires riverine isotopic composition to be much lower than any observed natural substance [*Stirling et al.*, 2007; *Weyer et al.*, 2008; *Tissot and Dauphas*, 2015], making this scenario highly improbable. Given a more reasonable $\delta_{riv}$ value (–0.27‰ for modern [*Noordmann et al.*, 2015; *Andersen et al.*, 2016]), decreasing $F_{riv}$ could also generate a negative excursion in $\delta^{238}$U. However, even decreasing this flux to zero results in changes to $\delta^{238}$U and [U] that are very gradual and thus are too small to measure with existing instrument precision and far smaller than observed variation. This model result occurs largely because decreasing $F_{riv}$ causes seawater [U] to decrease, which in turn decreases both of the uranium outfluxes, which are each proportional to [U]. Thus, the residence time of uranium increases significantly, and only a small decrease in $\delta^{238}$U occurs with the modeled time interval.

Additionally, these alternative scenarios are not consistent with existing evidence for an expansion in marine anoxia [*van de Schootbrugge et al.*, 2013; *Kasprak et al.*, 2015]. Given the existing evidence for expanded anoxia from other sources of data, we argue that an expansion in anoxia is the most parsimonious explanation for the first order patterns in $\delta^{238}$U and that higher order

variations in $\delta^{238}$U are due to U(IV) incorporation, increased uranium delivery via continental weathering, and variations in the proportions of aragonite in the original carbonate sediment. It is challenging to determine the appropriate seawater $\delta^{238}$U value to assume at steady state. In general, our modeling suggests that anoxia expanded anywhere from 40 to 100-fold, which is similar or slightly smaller in magnitude that the change observed for the Early Triassic [*Brennecka et al*., 2011a; *Lau et al*., 2016]. Subsequent $\delta^{238}$U measurements from geographically distinct Late Triassic and Early Jurassic localities will help elucidate baseline $\delta^{238}$U seawater values.

### 5.3. Implications for the Biotic Recovery From the End-Triassic Extinction

Based on the data from northern Italy, acidification and anoxia appear to have initiated at the start of the end-Triassic extinction. Acidification was likely limited to the N1 excursion interval [*Jost et al*., 2017] (~25 kyr), whereas anoxia appears to have persisted until at least the peak of the P2 carbon isotope excursion (~45 kyr). This difference in duration of acidification versus anoxia suggests that the synergistic effects of acidification and anoxia were maximized near the onset of the extinction event, when most extinctions occurred, and that anoxia persisted longer into the Hettangian and possibly delayed biotic recovery. A carbonate reef gap extends for ~250 kyr into the Hettangian (until the *A. liasicus zone*) [*Kiessling et al*., 2007; *Ruhl et al*., 2010; *Martindale et al*., 2012, and references therein] and other marine animals did not recover until mid-Hettangian time [*Hallam*, 1996]. However, our modeling suggests that expanded anoxia persisted for less than 50 kyr, which implies that anoxic conditions would not have actively suppressed biodiversity for the entire duration of the recovery.

Our model assumes that the anoxic extent increased and decreased instantaneously, but it is possible that the extent of anoxia decreased gradually over 200 kyr from its acme. We simulate this scenario in an additional model run by stepping down anoxia from an initial high between 40 and 100-fold (depending on

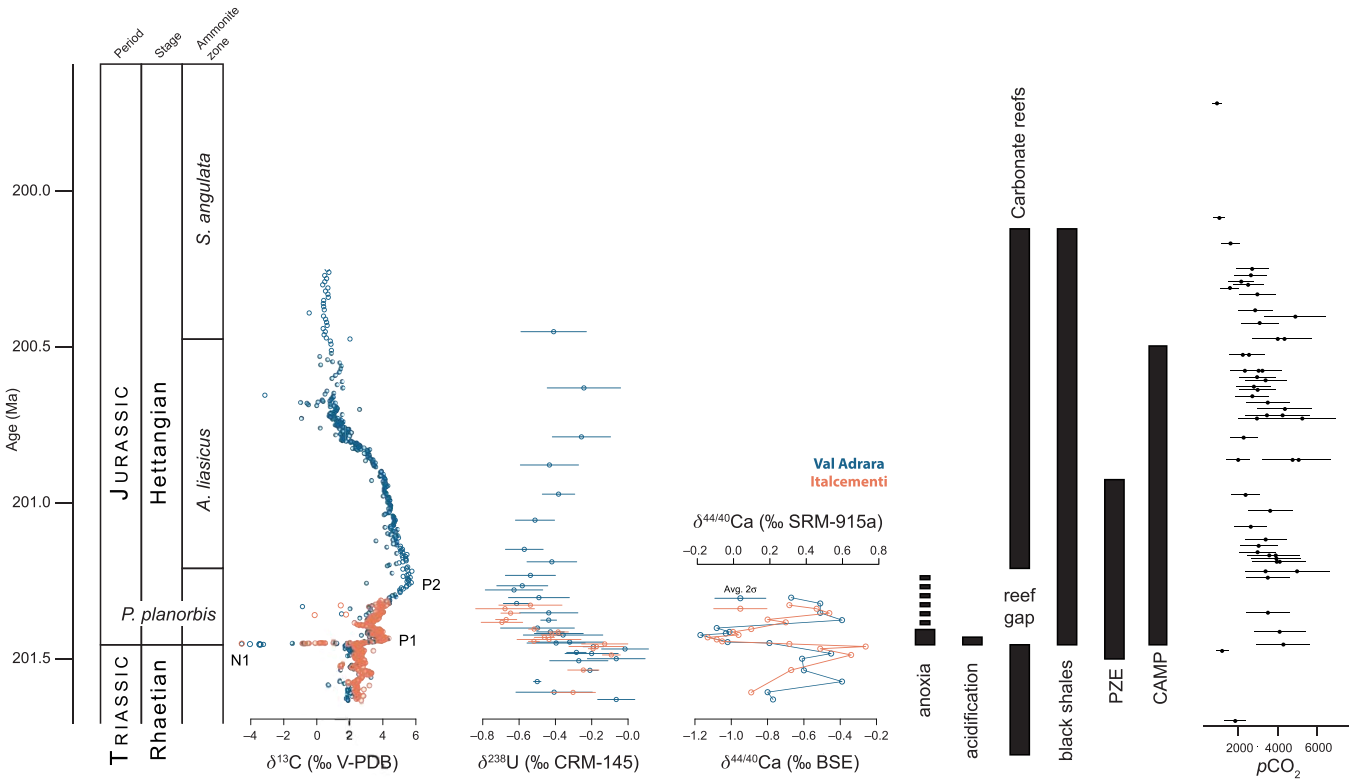


**Figure 8.** Summary of the temporal relationships between the records of $\delta^{13}$C, $\delta^{13}$C, and $\delta^{44/40}$Ca [*Jost et al*., 2017] from Val Adrara and Italcementi, model predictions for the duration of anoxia and acidification [*Jost et al*., 2017], the presence of carbonate reefs [*Kiessling et al*., 2009; *Martindale et al*., 2012], black shales [*van de Schootbrugge et al*., 2013], photic zone euxinia (PZE) [*Richoz et al*., 2012; *Kasprak et al*., 2015], and CAMP volcanism [*Schaller et al*., 2012; *Blackburn et al*., 2013], and $pCO_2$ [*Schaller et al*., 2011]. Ammonite zonation based on *Ruhl et al*. [2010].

model conditions) over 44 kyr to between 3 and 30-fold higher than initial conditions for the next 200 kyr (Figure 7). Most model scenarios predict values that match our observed $\delta^{238}$U and [U] records within error, though some fits are better than others. The small number of data points and the error on our $\delta^{238}$U data preclude a precise quantification of a gradual decrease in anoxia; however, these results demonstrate that it is plausible for anoxia to have lasted until the return of reefs and other marine animals.

Uranium isotope evidence for extensive and protracted bottom water anoxia during Hettangian time strengthens the case for a suite of environmental feedbacks between the carbon cycle and the biosphere as key controls on the dynamics of biotic recovery. Carbon release from CAMP and the associated warming can account for the timing of the mass extinction as well as the associated negative carbon isotope excursion (Figure 8). The initial carbon release event can also explain calcium isotope evidence for short-lived ocean acidification and a shift from calcite to aragonite deposition during acidification recovery [*Jost et al*., 2017], as well as uranium isotope evidence for expanded anoxia as a consequence of higher temperatures and increased weathering and eutrophication under high atmospheric $pCO_2$. The broad correspondence between the negative excursion in $\delta^{238}$U and elevated $pCO_2$ further points toward a climatic control on marine redox conditions, and the coincidence of the negative $\delta^{238}$U excursion and positive $\delta^{13}$C excursion implies that high rates of organic carbon export were associated with anoxic conditions. Expanded deposition of black shales [*van de Schootbrugge et al*., 2013] and the presence of biomarkers for photic zone euxinia [*Richoz et al*., 2012; *Kasprak et al*., 2015] provides further basin-scale geological corroboration of the isotopic evidence for global anoxia. The return of reef ecosystems likewise post-dates any evidence for acidification as well as the interval most likely affected by severe and extensive bottom water anoxia. In summary, carbon release from CAMP can account for the suite of biological and environmental disturbances that begin across the Triassic-Jurassic transition, and the waning of carbon release likewise explains the stabilization of biogeochemical cycles and recovery of marine animal ecosystems in the later Hettangian.

## 6. Conclusions

We observe a negative $\sim 0.7‰$ negative excursion in the $\delta^{238}$U of marine carbonates just above the T/J boundary. Modeling of the uranium cycle demonstrates that the pattern of uranium isotope variation is best explained through an expansion in anoxic uranium deposition in the earliest Jurassic. Although in situ reduction and fractionation of uranium in pore waters has been observed to increase the bulk $\delta^{238}$U composition of marine carbonate rocks, our data cannot be explained through this mechanism alone and must reflect secular changes in seawater $\delta^{238}$U. Some data, particularly from the uppermost Triassic, were likely influenced by incorporation of reduced U, but the effect appears to be smaller than the effect of anoxia. An increase in the weathering of uranium and a higher abundance of aragonite in the earliest Jurassic may have also impacted the data to a small degree.

Our observations are compatible with existing evidence for marine anoxia during the end-Triassic and follows predictions for increased weathering after a rapid rise in atmospheric $pCO_2$. Given that expansion of anoxic conditions coincides with the beginning of the end-Triassic extinction event and persists at least until the peak of the P2 carbon isotope excursion, anoxia had the potential to negatively impact biodiversity and delay the recovery of marine animals until mid-Hettangian time.

**Acknowledgments**
This study was supported in part by funds from AAPG, GSA, the Paleontological Society, and Stanford University to A.B.J. We thank G. Li for assistance in the laboratory, and Maya Elrick for her constructive review. All geochemical data produced in this study are presented in Table 1 of this manuscript. Additional carbon and calcium isotope data can be found in *Bachan et al*. [2012, 2014] and *Jost et al*. [2017].

## References

Andersen, M. B., S. Romaniello, D. Vance, S. H. Little, R. Herdman, and T. W. Lyons (2014), A modern framework for the interpretation of $^{238}U/^{235}U$ in studies of ancient ocean redox, *Earth Planet. Sci. Lett.*, *400*, 184–194, doi:10.1016/j.epsl.2014.05.051.

Andersen, M. B., D. Vance, J. L. Morford, E. Bura-naki, S. F. M. Breitenbach, and L. Och (2016), Closing in on the marine $^{238}U/^{235}U$ budget, *Chem. Geol.*, *420*, 11–22, doi:10.1016/j.chemgeo.2015.10.041.

Andersen, M. B., C. H. Stirling, and S. Weyer (2017), Uranium isotope fractionation, *Rev. Mineral. Geochem.*, *82*, 799–850, doi:10.2138/rmg.2017.82.19.

Anderson, R. F., M. Q. Fleisher, and A. P. LeHuray (1989), Concentration, oxidation state, and particulate flux of uranium in the Black Sea, *Geochim. Cosmochim. Acta*, *53*(9), 2215–2224, doi:10.1016/0016-7037(89)90345-1.

Azmy, K., B. Kendall, U. Brand, S. Stouge, and G. W. Gordon (2015), Redox conditions across the Cambrian–Ordovician boundary: Elemental and isotopic signatures retained in the GSSP carbonates, *Palaeogeogr. Palaeoclimatol. Palaeoecol.*, *440*, 440–454, doi:10.1016/j.palaeo.2015.09.014.

Bachan, A., and J. L. Payne (2015), Modelling the impact of pulsed CAMP volcanism on pCO2 and $\delta$13C across the Triassic–Jurassic transition, *Geol. Mag.*, *153*, 1–19, doi:10.1017/S0016756815000126.

Bachan, A., B. van de Schootbrugge, J. Fiebig, C. A. McRoberts, G. Ciarapica, and J. L. Payne (2012), Carbon cycle dynamics following the end-Triassic mass extinction: Constraints from paired $\delta$13C carb and $\delta$13C org records, *Geochem. Geophys. Geosyst.*, *13*, Q09008, doi:10.1029/2012GC004150.

Bachan, A., B. van de Schootbrugge, and J. L. Payne (2014), The end-Triassic negative $\delta^{13}$C excursion: A lithologic test, *Palaeogeogr. Palaeoclimatol. Palaeoecol.*, *412*, 177–186, doi:10.1016/j.palaeo.2014.07.027.

Barnes, C. E., and J. K. Cochran (1990), Uranium removal in oceanic sediments and the oceanic U balance, *Earth Planet. Sci. Lett.*, *97*, 94–101.

Basu, A., R. A. Sanford, T. M. Johnson, C. C. Lundstrom, and F. E. Löffler (2014), Uranium isotopic fractionation factors during U(VI) reduction by bacterial isolates, *Geochim. Cosmochim. Acta*, *136*, 100–113, doi:10.1016/j.gca.2014.02.041.

Bijma, J., H. O. Pörtner, C. Yesson, and A. D. Rogers (2013), Climate change and the oceans—What does the future hold?, *Mar. Pollut. Bull.*, *74*(2), 495–505, doi:10.1016/j.marpolbul.2013.07.022.

Blackburn, T. J., P. E. Olsen, S. A. Bowring, N. M. McLean, D. V Kent, J. Puffer, G. McHone, E. T. Rasbury, and M. Et-Touhami (2013), Zircon U-Pb geochronology links the end-Triassic extinction with the Central Atlantic Magmatic Province, *Science*, *340*(6135), 941–945, doi:10.1126/science.1234204.

Brennecka, G. A., L. E. Borg, I. D. Hutcheon, M. A. Sharp, and A. D. Anbar (2010), Natural variations in uranium isotope ratios of uranium ore concentrates: Understanding the $^{238}$U/$^{235}$U fractionation mechanism, *Earth Planet. Sci. Lett.*, *291*(1–4), 228–233, doi:10.1016/j.epsl.2010.01.023.

Brennecka, G. A., A. D. Herrman, T. J. Algeo, and A. D. Anbar (2011a), Rapid expansion of oceanic anoxia immediately before the end-Permian mass extinction, *Proc. Natl. Acad. Sci. U. S. A.*, *108*, 17,631–17,634, doi:10.1073/pnas.1106039108/-/DCSupplemental.

Brennecka, G. A., L. E. Wasylenki, J. R. Bargar, S. Weyer, and A. D. Anbar (2011b), Uranium isotope fractionation during adsorption to Mn-oxyhydroxides, 45, 1370–1375.

Chen, X., S. J. Romaniello, A. D. Herrmann, L. E. Wasylenki, and A. D. Anbar (2016), Uranium isotope fractionation during coprecipitation with aragonite and calcite, *Geochim. Cosmochim. Acta*, *188*, 189–207, doi:10.1016/j.gca.2016.05.022.

Clapham, M. E., and J. L. Payne (2011), Acidification, anoxia, and extinction: A multiple logistic regression analysis of extinction selectivity during the Middle and Late Permian, *Geology*, *39*(11), 1059–1062, doi:10.1130/g32230.1.

Clark, S. K., and T. M. Johnson (2008), Effective isotopic fractionation factors for solute removal by reactive sediments: A laboratory microcosm and slurry study, *Environ. Sci. Technol.*, *42*(21), 7850–7855, doi:10.1021/es801814v.

Condon, D. J., N. Mclean, S. R. Noble, and S. A. Bowring (2010), Isotopic composition ($^{238}$U/$^{235}$U) of some commonly used uranium reference materials, *Geochim. Cosmochim. Acta*, *74*(24), 7127–7143, doi:10.1016/j.gca.2010.09.019.

Dahl, T. W., R. A. Boyle, D. E. Canfield, J. N. Connelly, B. C. Gill, T. M. Lenton, and M. Bizzarro (2014), Uranium isotopes distinguish two geochemically distinct stages during the later Cambrian SPICE event, *Earth Planet. Sci. Lett.*, *401*, 313–326, doi:10.1016/j.epsl.2014.05.043.

Deutsch, C., A. Ferrel, B. Seibel, H.-O. Portner, and R. B. Huey (2015), Climate change tightens a metabolic constraint on marine habitats, *Science*, *348*(6239), 1132–1135, doi:10.1126/science.aaa1605.

Djogić, R., and M. Branica (1991), Dissolved uranyl complexed species in artificial seawater, *Mar. Chem.*, *36*, 121–135.

Dunk, R. M., R. A. Mills, and W. J. Jenkins (2002), A reevaluation of the oceanic uranium budget for the Holocene, *Chem. Geol.*, *190*, 45–67.

Elrick, M., V. Polyak, T. J. Algeo, S. Romaniello, Y. Asmerom, A. D. Herrmann, A. D. Anbar, L. Zhao, and Z. Chen (2016), Global-ocean redox variation during the middle-late Permian through Early Triassic based on uranium isotope and Th/U trends of marine carbonates, *Geology*, *45*(2), 1–4, doi:10.1130/G38585.1.

Galli, M. T., F. Jadoul, S. M. Bernasconi, S. Cirilli, and H. Weissert (2007), Stratigraphy and palaeoenvironmental analysis of the Triassic–Jurassic transition in the western Southern Alps (Northern Italy), *Palaeogeogr. Palaeoclimatol. Palaeoecol.*, *244*(1–4), 52–70, doi:10.1016/j.palaeo.2006.06.023.

Goto, K. T., et al. (2014), Uranium isotope systematics of ferromanganese crusts in the Pacific Ocean: Implications for the marine $^{238}$U/$^{235}$U isotope system, *Geochim. Cosmochim. Acta*, *146*, 43–58, doi:10.1016/j.gca.2014.10.003.

Greene, S. E., R. C. Martindale, K. A. Ritterbush, D. J. Bottjer, F. A. Corsetti, and W. M. Berelson (2012), Recognising ocean acidification in deep time: An evaluation of the evidence for acidification across the Triassic-Jurassic boundary, *Earth Sci. Rev.*, *113*(1–2), 72–93, doi:10.1016/j.earscirev.2012.03.009.

Hallam, A. (1990), The end-Triassic mass extinction event, *Geol. Soc. Am. Spec. Pap.*, *247*, 577–584.

Hallam, A. (1996), Recovery of the marine fauna in Europe after the end-Triassic and Early Toarcian mass Extinctions, *Geol. Soc. London Spec. Publ.*, *102*(102), 231–236, doi:10.1144/GSL.SP.1996.001.01.16.

Hallam, A., and P. B. Wignall (2000), Facies changes across the Triassic-Jurassic boundary in Nevada, USA, *J. Geol. Soc. London*, *157*(1), 49–54, doi:10.1144/jgs.157.1.49.

Hallam, A., P. B. Wignall, J. R. Yin, and J. B. Riding (2000), An investigation into possible facies changes across the Triassic-Jurassic boundary in southern Tibet, *Sediment. Geol.*, *137*(3–4), 101–106, doi:10.1016/S0037-0738(00)00155-X.

Hautmann, M., M. J. Benton, and A. Tomašových (2008), Catastrophic ocean acidification at the Triassic-Jurassic boundary, *Neues Jahrb. für Geol. und Paläontologie Abhandlungen*, *249*(1), 119–127, doi:10.1127/0077-7749/2008/0249-0119.

Helly, J. J., and L. A. Levin (2004), Global distribution of naturally occurring marine hypoxia on continental margins, 51, 1159–1168, doi:10.1016/j.dsr.2004.03.009.

Henderson, G. M., and R. F. Anderson (2003), The U-series toolbox for paleoceanography, *Rev. Mineral. Geochem.*, *52*(1), 493–531, doi:10.2113/0520493.

Hinojosa, J. L., C. M. Moy, C. A. Prior, T. I. Eglinton, C. P. McIntyre, C. H. Stirling, and G. S. Wilson (2015), Investigating the influence of regional climate and oceanography on marine radiocarbon reservoir ages in southwest New Zealand, *Estuarine Coastal Shelf Sci.*, *167*, 526–539, doi:10.1016/j.ecss.2015.11.003.

Holmden, C., M. Amini, and R. Francois (2015), Uranium isotope fractionation in Saanich Inlet: A modern analog study of a paleoredox tracer, *Geochim. Cosmochim. Acta*, *153*, 202–215, doi:10.1016/j.gca.2014.11.012.

Hood, A. S., N. J. Planavsky, M. W. Wallace, X. Wang, E. J. Bellefroid, B. Gueguen, and D. B. Cole (2016), Integrated geochemical-petrographic insights from component-selective d 238U of Cryogenian marine carbonates, 44(11), 935–938, doi:10.1130/G38533.1.

Jost, A. B., A. Bachan, B. van de Schootbrugge, S. T. Brown, D. J. DePaolo, and J. L. Payne (2017), Additive effects of acidification and mineralogy on calcium isotopes in Triassic/Jurassic boundary limestones, *Geochem. Geophys. Geosyst.*, *18*, 1–12, doi:10.1002/2016GC006724.

Kasprak, A. H., J. Sepulveda, R. Price-Waldman, K. H. Williford, S. D. Schoepfer, J. W. Haggart, P. D. Ward, R. E. Summons, and J. H. Whiteside (2015), Episodic photic zone euxinia in the northeastern Panthalassic Ocean during the end-Triassic extinction, *Geology*, *43*(4), 1–4, doi:10.1130/G36371.1.

Kiessling, W., and C. Simpson (2011), On the potential for ocean acidification to be a general cause of ancient reef crises, *Global Change Biology*, *17*(1), 56–67, doi:10.1111/j.1365-2486.2010.02204.x.

Kiessling, W., M. Aberhan, B. Brenneis, and P. J. Wagner (2007), Extinction trajectories of benthic organisms across the Triassic–Jurassic boundary, *Palaeogeogr. Palaeoclimatol. Palaeoecol.*, *244*(1–4), 201–222, doi:10.1016/j.palaeo.2006.06.029.

Kiessling, W., E. Roniewicz, L. Villier, P. Leonide, and U. Struck (2009), An early Hettangian coral reef in southern France: Implications for the end-Triassic reef crisis, *Palaios*, *24*(10), 657–671, doi:10.2110/palo.2009.p09-030r.

Knoll, A. H., R. K. Bambach, J. L. Payne, S. Pruss, and W. W. Fischer (2007), Paleophysiology and end-Permian mass extinction, *Earth Planet. Sci. Lett.*, *256*(3–4), 295–313, doi:10.1016/j.epsl.2007.02.018.

Lau, K. V., K. Maher, D. Altiner, B. M. Kelley, L. R. Kump, D. J. Lehrmann, J. C. Silva-Tamayo, K. L. Weaver, M. Yu, and J. L. Payne (2016), Marine anoxia and delayed Earth system recovery after the end-Permian extinction, *Proc. Natl. Acad. Sci. U. S. A.*, *113*(9), 2360–2365, doi:10.1073/pnas.1515080113.

Lau, K. V, F. A. Macdonald, K. Maher, and J. L. Payne (2017), Uranium isotope evidence for temporary ocean oxygenation in the aftermath of the Sturtian Snowball Earth, *Earth Planet. Sci. Lett.*, *458*, 282–292, doi:10.1016/j.epsl.2016.10.043.

Maher, K., J. R. Bargar, and G. E. Brown (2013), Environmental speciation of actinides, *Inorg. Chem.*, *52*(7), 3510–3532, doi:10.1021/ic301686d.

Martindale, R. C., W. M. Berelson, F. A. Corsetti, D. J. Bottjer, and A. J. West (2012), Constraining carbonate chemistry at a potential ocean acidification event (the Triassic–Jurassic boundary) using the presence of corals and coral reefs in the fossil record, *Palaeogeogr. Palaeoclimatol. Palaeoecol.*, *350–352*, 114–123, doi:10.1016/j.palaeo.2012.06.020.

McRoberts, C. A., H. Furrer, and D. S. Jones (1997), Palaeoenvironmental interpretation of a Triassic-Jurassic boundary section from western Austria based on palaeoecological and geochemical data, *Palaeogeogr. Palaeoclimatol. Palaeoecol.*, *136*(1–4), 79–95, doi:10.1016/S0031-0182(97)00074-6.

Meyer, K. M., and L. R. Kump (2008), Oceanic euxinia in earth history: Causes and consequences, *Annu. Rev. Earth Planet. Sci.*, *36*(1), 251–288, doi:10.1146/annurev.earth.36.031207.124256.

Morford, J. L., and S. Emerson (1999), The geochemistry of redox sensitive trace metals in sediments, *Geochim. Cosmochim. Acta*, *63*, 1735–1750.

Noordmann, J., S. Weyer, R. B. Georg, and M. Sharma (2015), Isotopes in environmental and health studies U/U isotope ratios of crustal material, rivers and products of hydrothermal alteration: New insights on the oceanic U isotope mass balance, 52, 37–41, doi:10.1080/10256016.2015.1047449.

Payne, J. L., and M. E. Clapham (2012), End-Permian mass extinction in the oceans: An ancient analog for the twenty-first century?, *Annu. Rev. Earth Planet. Sci.*, *2012*, 89–111, doi:10.1146/annurev-earth-042711-105329.

Pörtner, H. O., M. Langenbuch, and A. Reipschlager (2004), Biological impact of elevated $CO_2$ concentrations: Lessons from animal physiology and earth history?, *J. Oceanogr.*, *60*(4), 705–718.

Reeder, R. J., M. Nugent, G. M. Lamble, C. D. Tait, and D. E. Morris (2000), Uranyl incorporation into calcite and aragonite: XAFS and luminescence studies, *Environ. Sci. Technol.*, *34*, 638–644.

Reeder, R. J., E. J. Elzinga, C. D. Tait, K. D. Rector, R. J. Donohoe, and D. E. Morris (2004), Site-specific incorporation of uranyl carbonate species at the calcite surface, *Geochim. Cosmochim. Acta*, *68*(23), 4799–4808, doi:10.1016/j.gca.2004.05.031.

Richoz, S., et al. (2012), Hydrogen sulphide poisoning of shallow seas following the end-Triassic extinction, *Nat. Geosci.*, *5*(9), 662–667, doi:10.1038/ngeo1539.

Romaniello, S. J., A. D. Herrmann, and A. D. Anbar (2013), Uranium concentrations and $^{238}U/^{235}U$ isotope ratios in modern carbonates from the Bahamas: Assessing a novel paleoredox proxy, *Chem. Geol.*, *362*, 305–316, doi:10.1016/j.chemgeo.2013.10.002.

Ruhl, M., M. H. L. Deenen, H. A. Abels, N. R. Bonis, W. Krijgsman, and W. M. Kürschner (2010), Astronomical constraints on the duration of the early Jurassic Hettangian stage and recovery rates following the end-Triassic mass extinction (St Audrie's Bay/East Quantoxhead, UK), *Earth Planet. Sci. Lett.*, *295*(1–2), 262–276, doi:10.1016/j.epsl.2010.04.008.

Schaller, M. F., J. D. Wright, and D. V Kent (2011), Atmospheric $PCO_2$ perturbations associated with the Central Atlantic Magmatic Province, *Science*, *331*(6023), 1404–1409, doi:10.1126/science.1199011.

Schaller, M. F., J. D. Wright, D. V. Kent, and P. E. Olsen (2012), Rapid emplacement of the Central Atlantic Magmatic Province as a net sink for $CO_2$, *Earth Planet. Sci. Lett.*, *323–324*, 27–39, doi:10.1016/j.epsl.2011.12.028.

Schauble, E. (2007), Role of nuclear volume in driving equilibrium stable isotope fractionation of mercury, thallium, and other very heavy elements, *Geochim. Cosmochim. Acta*, *71*(9), 2170–2189, doi:10.1016/j.gca.2007.02.004.

Stirling, C. H., M. B. Andersen, E.-K. Potter, and A. N. Halliday (2007), Low-temperature isotopic fractionation of uranium, *Earth Planet. Sci. Lett.*, *264*(1–2), 208–225, doi:10.1016/j.epsl.2007.09.019.

Stirling, C. H., M. B. Andersen, R. Warthmann, and A. N. Halliday (2015), Isotope fractionation of $^{238}U$ and $^{235}U$ during biologically-mediated uranium reduction, *Geochim. Cosmochim. Acta*, *163*, 200–218, doi:10.1016/j.gca.2015.03.017.

Stylo, M., N. Neubert, Y. Wang, N. Monga, S. J. Romaniello, S. Weyer, and R. Bernier-Latmani (2015), Uranium isotopes fingerprint biotic reduction, *Proc. Natl. Acad. Sci. U. S. A.*, *112*(18), 5619–5624, doi:10.1073/pnas.1421841112.

Tissot, F. L. H., and N. Dauphas (2015), Uranium isotopic compositions of the crust and ocean: Age corrections, U budget and global extent of modern anoxia, *Geochim. Cosmochim. Acta*, *167*, 113–143, doi:10.1016/j.gca.2015.06.034.

van de Schootbrugge, B., and P. B. Wignall (2015), A tale of two extinctions: Converging end-Permian and end-Triassic scenarios, *Geol. Mag.*, *153*, 332–354, doi:10.1017/S0016756815000643.

van de Schootbrugge, B., J. L. Payne, A. Tomasovych, J. Pross, J. Fiebig, M. Benbrahim, K. B. Föllmi, and T. M. Quan (2008), Carbon cycle perturbation and stabilization in the wake of the Triassic-Jurassic boundary mass-extinction event, *Geochem. Geophys. Geosyst.*, *9*, Q04028, doi:10.1029/2007GC001914.

van de Schootbrugge, B., A. Bachan, G. Suan, S. Richoz, and J. L. Payne (2013), Microbes, mud and methane: cause and consequence of recurrent Early Jurassic anoxia following the end-Triassic mass extinction, *Palaeontology*, *56*(4), 685–709, doi:10.1111/pala.12034.

Weyer, S., A. Anbar, A. Gerdes, G. Gordon, T. Algeo, and E. Boyle (2008), Natural fractionation of $^{238}U/^{235}U$, *Geochim. Cosmochim. Acta*, *72*(2), 345–359, doi:10.1016/j.gca.2007.11.012.

Wignall, P. B., J. P. Zonneveld, R. J. Newton, K. Amor, M. A. Sephton, and S. Hartley (2007), The end Triassic mass extinction record of Williston Lake, British Columbia, *Palaeogeogr. Palaeoclimatol. Palaeoecol.*, *253*(3–4), 385–406, doi:10.1016/j.palaeo.2007.06.020.